Citation: **Hirt, C**. (2014), GOCE's view below the ice of Antarctica: Satellite gravimetry confirms improvements in Bedmap2 bedrock knowledge, Geophysical Research Letters 41(14), 5021-5028, doi: 10.1002/2014GL060636.

GOCE's view below the ice of Antarctica: Satellite gravimetry confirms improvements in Bedmap2 bedrock knowledge

Christian Hirt

Western Australian Centre for Geodesy & The Institute for Geoscience Research, Curtin University, GPO Box U1987, Perth, WA 6845, Australia
Email: c.hirt@curtin.edu.au
Currently at: Institute for Astronomical and Physical Geodesy & Institute for Advanced Study Technische Universität München, Germany

Key points

- GOCE satellite gravity is used to evaluate gravity implied by Bedmap2 masses
- Gravity from GOCE and Bedmap2 in good agreement to 80 km spatial scales
- Evidence of GOCE's sensitivity for subsurface mass distribution over Antarctica

Key words

GOCE, satellite gravity, bedrock, topography, gravity forward modelling

Abstract

Accurate knowledge of Antarctica's topography, bedrock and ice sheet thickness is pivotal for climate change and geoscience research. Building on recent significant progress made in satellite gravity mapping with ESA's GOCE mission, we here reverse the widely used approach of validating satellite gravity with topography and instead utilize the new GOCE gravity maps for novel evaluation of Bedmap1/2. Space-collected GOCE gravity reveals clear improvements in the Bedmap2 ice and bedrock data over Bedmap1 via forward-modelled topographic mass and gravity effects at spatial scales of 400 to 80 km. Our study demonstrates GOCE's sensitivity for the subsurface mass distribution in the lithosphere, and delivers independent evidence for Bedmap2's improved quality reflecting new radar-derived ice thickness data. GOCE and Bedmap2 are combined to produce improved Bouguer gravity maps over Antarctica. We recommend incorporation of Bedmap2 in future high-resolution global topography and geopotential models, and its use for detailed geoid modelling over Antarctica.

Index Terms 1240 (Satellite geodesy: results), 1214 (Geopotential theory and determination), 1219 (Gravity anomalies and Earth structure), 0738 (Ice), 7218 (Lithosphere)

Keywords GOCE, gravity, forward modelling, Bedmap1, Bedmap2

1 Introduction

Reliable and accurate models of the surface topography, ice sheet thickness and bedrock topography, i.e. rock covered by ice sheets, are salient for geoscience and climate change research over the Antarctic continent [e.g., *Shepherd et al.,* 2012]. Such data compilations support geological, tectonic and geophysical data interpretation, and provide valuable boundary conditions in modelling Glacial Isostatic Adjustment processes [e.g., *Ivins and James,* 2005], ice sheet evolution and ice flow behaviour. With the release of Bedmap2 [*Fretwell et al.*, 2013], a new set of gridded data has become available to the scientific community which describes in a self-consistent manner ice sheet thickness, surface- and bedrock topography. Based on a new ice thickness data base which is substantially (about ten times) larger than that of its predecessor Bedmap1 [*Lythe et al.*, 2001], Bedmap2 resolves the bed structure beneath Antarctica's ice sheets with finer detail than before [*Fretwell et al.,* 2013].

Significant advancements in high-resolution mapping of Earth's static gravity field from space have now been made with European Space Agency (ESA)'s Gravity field and Ocean Circulation Explorer (GOCE) satellite [*Drinkwater et al.*, 2003; *Rummel et al*., 2011]. During its four-year mission phase, GOCE has delivered high-precision gravity gradient and orbit trajectory data that has been used as input for the computation of a series of new global gravity models with up to ~80 km spatial resolution [*Pail et al.,* 2011].

Given that the topographic masses greatly shape a planet's gravitational field, high-resolution topography models are frequently used in planetary sciences to assess the quality of space-collected gravity models. Examples include gravity fields for Moon [*Lemoine et al.,* 2014], Mars [*Konopliv et al.*, 2011], and Earth [*Hirt et al*., 2012]. Strong agreement between the gravity model and the mostly much better resolved topography is taken as an indicator for the gravity model's quality, particularly at shorter spatial scales [e.g., *Goossens et al.,* 2011].

Here we reverse the standard approach of evaluating-gravity-with-topography and deploy new high-resolution GOCE gravity to provide independent evidence for significant improvements in Antarctic bedrock data. This is a new application of satellite gravimetry, and complementary to its routine use for mass-change detection over ice sheets, e.g., *Shepherd et al.* [2012]. Our letter unites recent progress in the field of space gravity observation, gravity forward-modelling and topographic mass modelling over Antarctica. We use the 2013 GOCE gravity field model TIM4 [*Pail et al.,* 2011] as source of new gravity information over Antarctica with 80 km spatial resolution for a novel evaluation of Bedmap2, also relative to its predecessor Bedmap1 [*Lythe et al.*, 2001] and global topography data, Sect. 2.

Bedmap2 information on the geometry of rock, water and ice masses is processed in spherical harmonics applying a recent approach for gravity forward modelling in the spectral domain [*Claessens and Hirt*, 2013]. Rigorously accounting for Earth's ellipsoidal shape in the forward modelling, this approach delivers Bedmap2's topographic potential (i.e., gravitational potential derived from the Bedmap2 topography) in ellipsoidal representation which is 'compatible' with GOCE gravity models (Sect. 3). Comparisons between gravity derived from both Bedmap releases and independent GOCE gravity provide external evidence for improved bedrock representation in Bedmap2 (Sect. 4.1), while demonstrating GOCE's sensitivity for subsurface mass-density anomalies. The results have implications for the interpretation of recent gravity maps (Sect. 4.2), for the development of new high-resolution global gravity and topography models, and for high-resolution modelling of Antarctica's gravity field (Sect. 5).

2 Data

2.1 GOCE gravimetry

ESA's GOCE satellite mission has determined Earth's static gravity field during a ~4 year data collection period (from 2009 to 2013) using a dedicated gravity gradiometer for the measurement of second derivatives of the gravitational potential at ~260 km altitude [*Rummel et al.*, 2011; *van der Meijde et al.*, 2013]. As a second major measurement system, GPS-based satellite-to-satellite tracking was deployed aboard the GOCE satellite for orbit determination, augmenting the gradiometer observations in the long-wavelengths. During the life-time of the GOCE mission, ESA has computed and released 10 different spherical harmonic gravity models from the GOCE gradiometer and GPS orbit data. From these gravity models – which differ in the processing strategies applied and amount of data used [cf. *van der Meijde et al*., 2013] – we use the latest GOCE gravity field model computed with the time-wise approach (TIM4), cf. *Pail et al.* [2011]. TIM4 is a GOCE-only gravity field based on the first 31.5 months of mission data. It reaches an accuracy of ~1mGal for gravity anomalies at ~100 km spatial scales or spherical harmonic degree 200 [*van der Meijde et al.*, 2013], while partially resolving the gravity field down to ~80 km scales (or harmonic degree 250), also see Sect. 4.

2.2 Bedmap2 and Bedmap1

Bedmap2 [*Fretwell et al.*, 2013] describes Antarctica's surface topography, bedrock beneath ice, surrounding seafloor, and thicknesses of grounded ice sheets and floating ice shelves at 1 arc-min spatial resolution between 60° and 90° South latitude. While the Bedmap2 surface topography has been measured predominantly through satellite radar altimetry with great detail and completeness over large parts of Antarctica, information on ice sheet thickness and bedrock topography is sourced from regional or local surveys of incomplete continental coverage. In Bedmap2, direct measurements for ice thicknesses and bedrock topography are primarily from airborne ice-penetrating radar soundings, but also from seismic surveys. According to *Fretwell et al.*, [2013], about 36% (83%) of grid-points at 5 km (20 km) resolution are constrained by direct measurements, which is a substantial increase over Bedmap1 where only 17% of cells are constrained at 5 km resolution. Importantly, Bedmap2 contains ice thickness data indirectly determined through inversion of 2010 GOCE satellite gravimetry [*Fretwell et al*., 2013] over areas of Antarctica devoid of direct ice sheet measurements (that is, more than 50 km distance to nearest measurement). These areas are excluded in our numerical study to ensure independence among GOCE and Bedmap2 (cf. Sect. 3.5 and 4).

Table 1. Sources of surface topography (surface), bedrock topography (bed) and ice sheet thicknesses (ice) for generation of Bedmap2 and Bedmap1 implied gravity.

Case	Component	South of -60° latitude	North of -60° latitude
(a) Bedmap2	Surface	Bedmap2 topography	ETOPO1 topography
	Bed	Bedmap2 bedrock	ETOPO1 bedrock
	Ice	Bedmap2 ice thickness	ETOPO1 topography- bedrock
(b) Bedmap1	Surface	ETOPO1 topography*1	ETOPO1 topography
	Bed	ETOPO1 bedrock*2	ETOPO1 bedrock
	Ice	ETOPO1 topography- bedrock	ETOPO1 topography- bedrock

*1 RAMP topography (2001) by National Snow and Ice Data Centre

*2 Bedmap1 bedrock [*Lythe et al*., 2001]

2.3 Global topography models

The spherical harmonic methods applied in this study require models of Earth's global topography rather than over Antarctica only. We have chosen the widely used ETOPO1 [*Amante and Eakins*, 2009] 1 arc-min global topography and bedrock model as supporting data source for extending Bedmap2 North of 60° South latitude. Composed of a multitude of data sources, ETOPO1 mainly contains SRTM topography over land, GEBCO bathymetry over the oceans, and importantly Bedmap1 bedrock over Antarctica [cf. *Amante and Eakins,* 2009]. In order to test the performance of Bedmap2 and Bedmap1 in a comparative manner, we use (a) a merger of Bedmap2 and ETOPO1, and (b) ETOPO1-only as source of Bedmap1 bedrock data (Table 1).

3 Methods

3.1 Rock equivalent topography

Bedmap2 provides information on the upper and lower boundaries of ice sheets and water bodies, and of the bedrock geometry (Fig. 1). Combined with mass-density assumptions of ice (ρ_I=917 kg m^{-3}), water (oceans: ρ_O=1030 kg m^{-3}, subglacial lakes: ρ_L=1000 kg m^{-3}), and topographic rock (ρ_R=2670 kg m^{-3}), we use Bedmap2 to define three-dimensional mass bodies. The water and ice mass bodies are numerically compressed into layers equivalent to topographic rock, which is in accordance with the widely used rock-equivalent topography (RET) concept [e.g., *Rummel et al.,* 1988; *Balmino et al.,* 2012]. While the geometry of the mass-bodies is changed, RET preserves the actual masses and allows working with a single constant mass-density of topographic rock ρ_R over all types of terrain. Depending on the type of terrain (Figure 1), we compute RET heights H_{RET} via:

$$H_{RET} = H_{BED} + \frac{\rho_O}{\rho_R}\Delta H_O \quad (1)$$

$$H_{RET} = H_{BED} + \frac{\rho_I}{\rho_R}\Delta H_I \quad (2)$$

$$H_{RET} = H_{BED} + \frac{\rho_O}{\rho_R}\Delta H_O + \frac{\rho_I}{\rho_R}\Delta H_I \quad (3)$$

where H_{BED} is bedrock height, ΔH_O denotes the ocean water column height, and ΔH_I is the ice sheet thickness. Eq. (1) is used over the oceans, Eq. (2) over ice-covered land and Eq. (3) over ice shelves. Computation of RET over subglacial lake water is similar to the ice shelf case, however, with ρ_L used instead of ρ_O, and ΔH_L instead of ΔH_O in Eq. (3). Over ice-free land, $H_{RET} = H_{BED}$. The described RET procedure is applied inside and outside the Bedmap2 data area (Table 1). To test the Bedmap1 bedrock performance (Table 1) we created a second global latitude-longitude grid of H_{RET} solely based on ETOPO1.

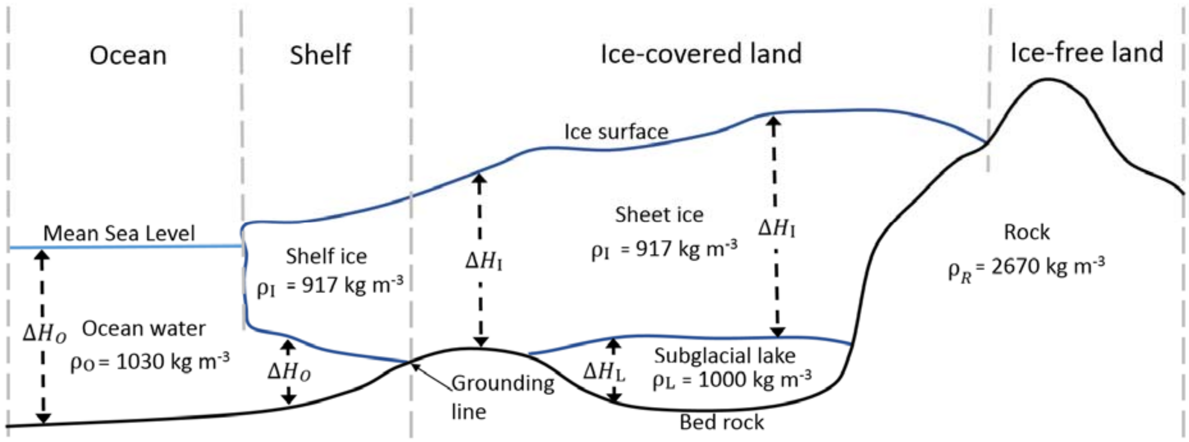

Fig. 1. Types of terrain over Antarctica, as extracted from Bedmap2 and used for construction of RET heights. Also shown are heights of water and ice columns, and mass-density values assigned in this study to (i) ocean water, (ii) subglacial water, (iii) ice and (iv) rock.

3.2 Topographic potential

The topographic potential of the masses, as represented by H_{RET} and the mass-density of topographic rock ρ_R, is computed with respect to the GRS80 reference ellipsoid [*Moritz*, 2000] in spherical harmonics. We use the harmonic combination method of *Claessens and Hirt* [2013] which is a gravity forward modelling (GFM) technique that expands the topographic potential into integer powers of H_{RET} relative to the GRS80 ellipsoid. We follow exactly the procedure described in *Claessens and Hirt* [2013] to derive fully-normalized topographic potential coefficients ($\overline{VC}_{nm}, \overline{VS}_{nm}$) to harmonic degree *n* and order *m* 2190, whereby the GRS80 numerical values *GM* (Gravitational Constant times Earth's mass) and *a* (semi-major axis) define the model constants. Two sets of ($\overline{VC}_{nm}, \overline{VS}_{nm}$) coefficients were generated separately from the Bedmap2 and Bedmap1 RET grids, and are used here to degree 250 only which is commensurate with the GOCE model resolution. Compared to traditional spectral domain GFM methods [e.g., *Rummel et al.*,1988; *Balmino et al.*, 2012] that rely on a mass-sphere of some constant radius, the harmonic combination method yields the topographic potential relative to the GRS80 mass-ellipsoid (both methods 'map' topographic heights onto the surface of the reference body). This accounts for Earth's ellipsoidal shape, and delivers the topographic potential fully compatible with global geopotential models from the GOCE mission [*Claessens and Hirt*, 2013].

The heights H_{RET} are treated as uncompensated in this study, which is a simplification of reality where isostatic compensation counteracts the gravity effect of the topographic masses at longer spatial scales. While observed satellite gravity is sensitive to both effects, it remains a challenge to accurately and completely forward-model the compensation part – be it on the basis of hypotheses or crustal thickness models (see detailed results e.g., in *Hirt et al.*, [2012]). Recently published crustal thickness maps for Antarctica (e.g., *Baranov and Morelli*, [2013]) either lack sufficient resolution or depend on GOCE (*O'Donnell and Nyblade,* [2014]), so would not meaningfully enhance the forward-modelling in our study.

3.3 Gravity synthesis

The topographic potential coefficients ($\overline{VC}_{nm}, \overline{VS}_{nm}$) are used for the synthesis of gravity δg (technically gravity disturbances being the radial derivatives of the potential)

$$\delta g = \frac{GM}{r^2} \sum_{n1}^{n2} (n+1) \left(\frac{a}{r} \right)^n \sum_{m=0}^{n} (\overline{VC}_{nm} \cos m\lambda + \overline{VS}_{nm} \sin m\lambda) \overline{P}_{nm}(\sin\varphi) \qquad (4)$$

where (φ, λ, r) are the 3D coordinates of the evaluation point (λ longitude, φ geocentric latitude and r geocentric radius), $\overline{P}_{nm}(\sin\varphi)$ are the fully-normalized associated Legendre functions of degree *n* and order *m*, *GM* and *a* are the models constants, and n_1 (n_2) are the lower and upper harmonic degree defining the harmonic band of evaluation ($2 \leq n_1 \leq n_2 \leq 250$). Our evaluation points form regular 10 arc-min latitude-longitude grids at 4000 m height above the GRS80 reference ellipsoid, so are outside of the topographic masses. Eq. 4 is used separately for synthesis of Bedmap2-implied topographic gravity (denoted with δg_{BM2}), Bedmap1 (δg_{BM1}) and GOCE-TIM4 observed gravity (δg_{GOCE}) with the respective model coefficients and constants.

3.4 Indicators

Cross-comparisons between GOCE-observed gravity δg_{GOCE} and Bedmap2 (Bedmap1) topographic gravity $\delta g_{BM1,2}$ at different spatial scales allow identification of improvements in bedrock knowledge over Antarctica. As key indicators, we use cross-correlation coefficients (CCs)

$$CC = \frac{\sum \left(\delta g_{GOCE} - \overline{\delta g}_{GOCE} \right) \left(\delta g_{BM1,2} - \overline{\delta g}_{BM1,2} \right)}{\sqrt{\sum \left(\delta g_{GOCE} - \overline{\delta g}_{GOCE} \right)^2 \sum \left(\delta g_{BM1,2} - \overline{\delta g}_{BM1,2} \right)^2}} \qquad (5)$$

with the overbar denoting mean values, and the summation done over all data points, and reduction rates (RRs), *Hirt et al.* [2012]

$$RR = 100\% \left(1 - \frac{RMS(\delta g_{GOCE} - \delta g_{Bedmap1,2})}{RMS(\delta g_{Bedmap1,2})} \right) \qquad (6)$$

to quantify the agreement between GOCE satellite-collected and Bedmap1,2-implied topographic gravity. Both CCs and RRs allow cross-comparisons with geographic specificity (e.g., over Antarctica or selected parts thereof) and over different spectral bands of the gravity spectrum. In Eq. 6, RMS is the root-mean-square operator describing mean gravity signal strengths. RRs quantify the amount of topographic gravity captured by the GOCE gravity model. RRs were shown in *Hirt et al.* [2012] to be a useful indicator for the topographic evaluation of observed gravity fields. RRs around zero (or negative) indicate that spatial patterns and magnitudes of observed and topographic gravity are unrelated, while moderately positive RRs (say around ~30% or higher) are an indication for substantial topographic gravity signals 'explained' by the GOCE observation [*Hirt et al*., 2012]. Unknown mass density anomalies, unmodelled isostatic compensation effects, but also any kind of modelling deficiencies [e.g., *Papp*, 2009] cause residual gravity signals. These prevent RRs from reaching the theoretical maximum value of 100 % (cf. Eq. 6) in practice. While CCs indicate the similarity between gravity signal patterns, RRs quantify the similarity between gravity signal magnitudes too.

3.5 Definition of evaluation areas

GOCE-observed and Bedmap-implied topographic gravity were computed in a range of narrow spectral bands $[n_1 \;\; n_2]$ with band widths of 10 harmonic degrees over two different areas

- Area A: Continental Antarctica without surrounding open oceans, and without any area where Bedmap2 ice thickness was derived from inversion of GOCE satellite gravity,
- Area B: All continents and oceans without continental Antarctica.

Exclusion of GOCE-dependent Bedmap2 data cells in area A ensures independence between Bedmap2 and GOCE in the gravity comparisons (Bedmap2 cells derived through gravity inversion were identified based on Bedmap2 bed elevation uncertainty values of 1000 m, cf. *Fretwell et al.* [2013]). The role of Area B is to show the behaviour of our indicators globally. Importantly, evaluation points South (North) of -83.3° (83.3°) latitude, respectively, are not included in areas A and B. This is justified because GOCE did not directly map the gravity field over the poles due to its orbit inclination of 96.7°.

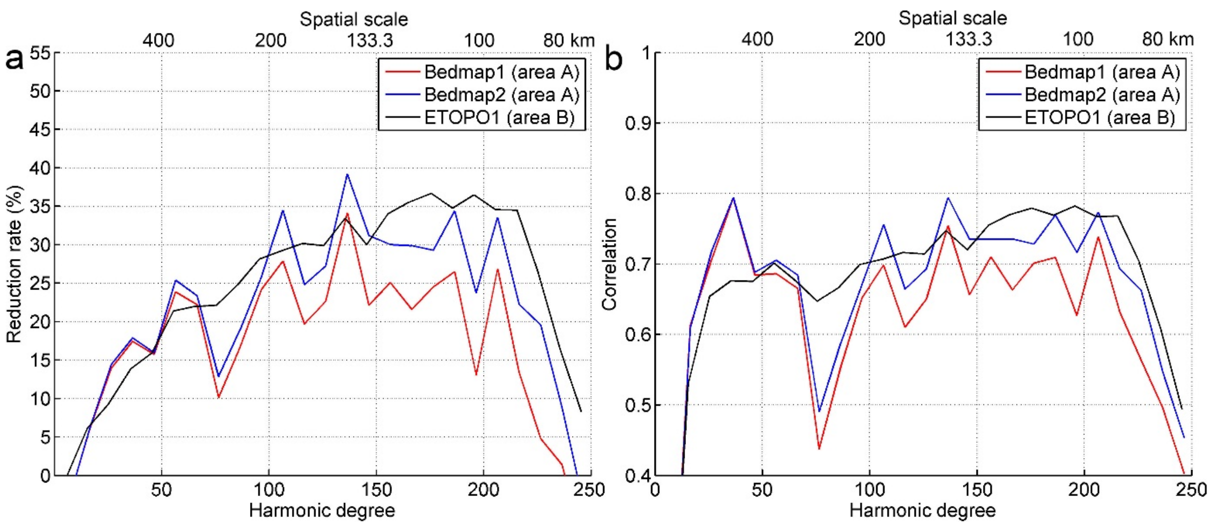

Fig. 2. Comparisons between GOCE-TIM 4 gravity and gravity implied by Bedmap1, Bedmap2 and global ETOPO1 topographic mass models. Left: Reduction rates RRs, right: correlation coefficients CC between GOCE gravity and the three topographic masses models. RRs and CCs shown as a function of the harmonic degree and spatial scale.

4 Results and discussion

4.1 Spectral analyses

CCs and RRs were computed from GOCE and Bedmap1,2 gravity over areas A and B in terms of spectral bands of 10 harmonic degrees width (Fig. 2). RRs are negative or near zero for the very long wavelengths of the gravity field (say n = 20), increase to maximum values (RRs around 25-35%) around $n \approx$ 100 to 210, before steadily dropping to ~5-10% around n = 241 to 250. Qualitatively, the ascending behaviour reflects an increase in signals generated by the (uncompensated) topographic masses and sensed by the GOCE satellite, while the drop beyond degree ~200 exhibits the resolution limits of the GOCE gravity fields.

From a comparison of RRs between GOCE/Bedmap1 (red curves) and GOCE/Bedmap2 (blue curves), comparable or higher RRs are obtained for Bedmap2 over the entire spectrum, with notably higher RRs from degree ~50 to 250 (spatial scales of 400 to 80 km). Bedmap2 RRs exceed those of Bedmap1 by 5-7 % in an absolute sense from degree ~100 and higher (Fig. 2a). In a relative sense this is a considerable improvement in RRs from Bedmap1 to Bedmap2 of 20-25%. Fig. 2 also shows that Bedmap2 RRs approach those of the near-global area B (which serves as a baseline) while Bedmap1 RRs fall significantly short of the global curve over most of the spectrum. From analysis of CCs (Fig. 2b), overall a similar behaviour is evident for Bedmap1 vs. Bedmap2. While the improvement in CCs from Bedmap1 to Bedmap2 is rather small in an absolute sense (about 0.05 over most of the spectrum), Bedmap2 CCs are found to be nearly comparable with CCs obtained near-globally (area B) for most spectral bands. Opposite to this, Bedmap1 offers lower correlation with GOCE than Bedmap2 or ETOPO1 globally.

Both indicators (Fig. 2a and 2b) reveal improved agreement between gravity from the GOCE satellite and gravity implied by the Bedmap2 topographic masses over Bedmap1. Bedmap2 CCs and RRs and those of the global topographic/bathymetric masses are similar over most of the spectrum, suggesting that the quality of Bedmap2 topography, ice and bedrock data has almost become comparable (though not identical) with that of global data. Conversely, the consistently poorer performance of Bedmap1 against GOCE corroborates the poorer quality of Bedmap1 [e.g, *Fretwell et al.*, 2013], with the lack of ice thickness data in Bedmap1 affecting at least at spatial scales the 400 to 80 km (Fig. 2). The similarity in RRs and CCs for both Bedmap releases at low harmonic degrees (say up to n = 50) suggests that the long-wavelength structure in Antarctic bedrock is already sufficiently represented in Bedmap1. Fig. 2 shows over the whole spectrum generally stronger oscillations in RRs and CCs for Bedmap1/2 (area A) than for ETOPO1 (area B). These are due to the limited extent of the regional areas, also see *Hirt et al.* [2012].

4.2 Bouguer gravity

To visualize the impact of Bedmap2 over Bedmap1 on gravity modelling and interpretation over Antarctica we have computed new Bouguer gravity maps by subtracting Bedmap-implied topographic gravity from GOCE-observed gravity:

$$\delta g_{Bouguer} = \delta g_{GOCE} - \delta g_{Bedmap1,2} \tag{6}$$

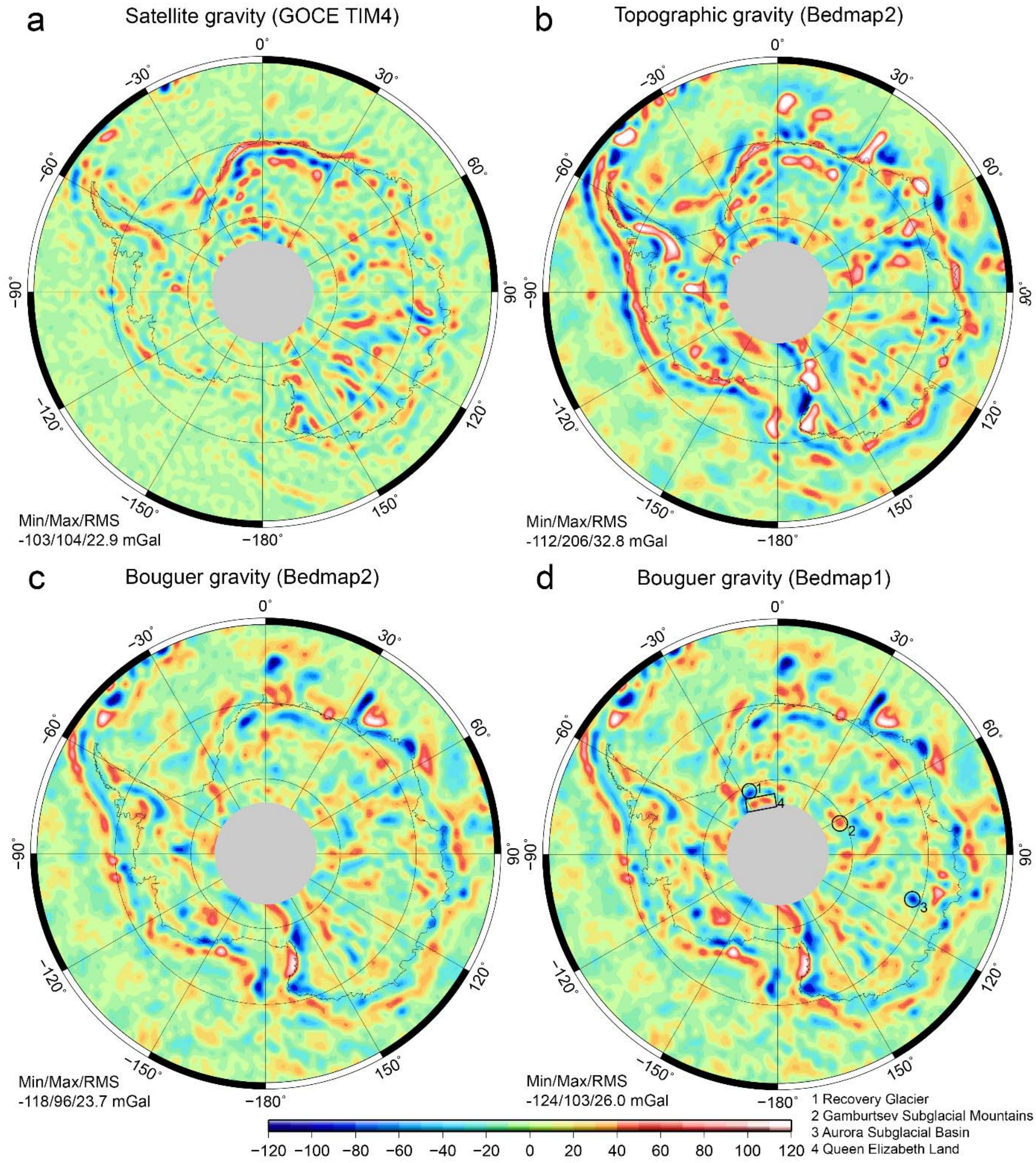

Fig. 3. GOCE, Bedmap and Bouguer gravity over Antarctica. A: GOCE gravity, B: Bedmap2 implied gravity, C: GOCE/Bedmap2 Bouguer gravity, D: GOCE/Bedmap1 Bouguer gravity. Shown are gravity disturbances. All gravity maps band-limited to harmonic degrees 50 to 220 (spatial scales of 400 to 80 km). The grey circle indicates the polar area not directly observed by GOCE. Statistics (Minimum/Maximum/Root-Mean-Square) computed over continental Antarctica, all units in mGal

Fig. 3a shows the GOCE-TIM4 gravity field and Fig. 3b Bedmap2-implied topographic gravity. Fig. 3c shows GOCE/Bedmap2, and for comparison purposes GOCE/Bedmap1 Bouguer gravity (Fig 3d). The gravity maps shown in Fig. 3 are in spherical harmonics and ellipsoidal approximation [*Claessens and Hirt* 2013] while being band-limited in spectral band of harmonic degrees 50 to 220. This is done in order to highlight the medium- and shortwavelength structure of the field at spatial scales of 400 to 80 km (see *Featherstone et al.*, 2013] for the benefits of the band limitation). From a visual comparison of the two Bouguer fields (Fig. 3c and 3d), an overall smoother and less variable field is obtained over the continent with Bedmap2 providing the topographic reduction (26.0 mGal RMS for Bedmap1 vs. 23.7 mGal RMS for Bedmap2 Bouguer gravity, cf. Figs. 3c and 3d). It is this smoothness that manifests itself in higher correlation (CCs) and signal reduction (RRs) for Bedmap2 in Fig. 2.

From comparison between Figs. 3b and 3c, the GOCE-observed gravity signal accounts for a substantial part of gravity implied by the Bedmap2 topographic masses (say around 30%, in terms of signal reduction). From comparison between Figs.3a and 3b, however, the signal strength of the (uncompensated) topographic gravity signal is significantly larger than that of the GOCE observation. This holds globally too, see the behaviour of potential power spectra in *Claessens and Hirt* [2013], Fig 5b ibid. This suggests a mixture of considerable compensation effects counteracting the topographic gravity signal and notable anomalous density structures in the upper crust, below the spatial domain modelled in Bedmap2.

Marked in Fig. 3d are four locations where the differences between the Bouguer maps, and thus Bedmap2 and Bedmap1 derived mass information, are distinct. These coincide with regions where the differences between Bedmap2 and Bedmap1 bedrock topography are maximum [*Fretwell et al.*, 2013, Fig .13]. Over these locations, Bouguer signals frequently reach amplitudes of ~50 mGal with Bedmap1 as reference, which are non-existent or less pronounced in the GOCE/Bedmap2 Bouguer maps. The much lower Bouguer signal amplitudes in Bedmap2 over these areas using GOCE as external benchmark indicates problem zones in Bedmap1 bedrock (locations 1,2,3 marked with circles in Fig. 3), while the smoothness in Bedmap2 Bouguer gravity over location 4 (marked with a rectangle) likely reflects dependencies with GOCE inverted ice-thicknesses. Given that Bedmap1 is a data source used for the ETOPO1 grids [*Amante and Eakins*, 2009], care should be exercised with the interpretation of ETOPO1-derived gravity maps, notably the World Gravity Map 2012 [WGM2012, *Bonvalot et al.*, 2012; *Balmino et al.*, 2012] over Antarctica, but also spherical harmonic topographic potential models based on the same data over Antarctica [*Grombein et al.*, 2014; *Claessens and Hirt*, 2013] released via the ICGEM gravity model service (http://icgem.gfz-potsdam.de/ICGEM/).

5 Conclusions

High-resolution gravity from the GOCE satellite gravimetry mission was used as external means to identify improvements in bedrock knowledge over Antarctica provided through the Bedmap2 grid collection. Relative to its predecessor Bedmap1, significant improvements could be detected in Bedmap2 bedrock knowledge at spatial scales of 400 to 80 km. In an absolute sense, the agreement between gravity from Bedmap2 and GOCE has come close to that between gravity from GOCE and Earth's global topography which is well known from space observation techniques. As such it is reasonable to conclude that the quality of Bedmap2 topography data is not much inferior to globally available topography data at the spatial scales investigated.

Bedmap2 bedrock topography and GOCE gravity data are valuable new data sources which will help improve Earth topography and gravity models over Antarctica and on a global scale.

Incorporation of Bedmap2 bedrock data is recommended into future ultra-high resolution global models of Earth's topography, e.g, as a follow-up to ETOPO1. On the gravity modelling side, GOCE, Bedmap2 and regional gravity [e.g., *Forsberg et al.,* 2011; *Schwabe et al.,* 2012] show promise for significant improvements over current geopotential models in use over Antarctica, which partially resolve the field not beyond ~100-110 km scales [e.g, EGM2008, *Pavlis et al.*, 2008]. The Bedmap2-contained information on bedrock and surface topography, and ice sheet thicknesses will also benefit ultra-high resolution gravity modelling initiatives [e.g. *Hirt et al*., 2013] in creating new detailed maps of gravity field functionals over the Antarctic continent.

Finally, GOCE's sensitivity for sensing gravity signals from subsurface masses, as shown for Antarctica's bedrock in this paper, is highly relevant in the context of lithosphere examinations based on GOCE [e.g., *O'Donnell and Nyblade*, 2014]. For Antarctica, inversion of latest-generation GOCE gravity models could provide better estimates of ice thicknesses [*Flury*, 2005] where no direct measurements are available.

Acknowledgements

I thank the Australian Research Council (ARC) for funding through discovery project grant DP120102441, and Technische Universität München (TUM) – Institute for Advanced Study (IAS) for partial support through the German Excellence Initiative and the European Union Seventh Framework Programme under grant agreement n° 291763.

References

Amante, C. and B. W. Eakins (2009), ETOPO1 1 Arc-Minute Global Relief Model: Procedures, Data Sources and Analysis. *NOAA Technical Memorandum* NESDIS NGDC-24, 19 pp, March 2009.

Balmino, G., Vales, N., Bonvalot, S., Briais, A. (2012), Spherical harmonic modelling to ultra-high degree of Bouguer and isostatic anomalies. *J Geod* 86(7):499-520. doi: 10.1007/s00190-011-0533.

Baranov, A and A. Morelli (2013), The Moho depth map of the Antarctica region, *Tectonophysics* 609, 299-313.

Bonvalot, S., Balmino, G., Briais, A., Kuhn, M., Peyrefitte, A., Vales, N., et al. (2012), World Gravity Map, 1:50,000,000 map, Eds.: BGI-CGMW-CNES-IRD, Paris.

Claessens S.J., C. Hirt (2013), Ellipsoidal topographic potential – new solutions for spectral forward gravity modelling of topography with respect to a reference ellipsoid, *Journal of Geophysical Research - Solid Earth*, 118(11), 5991-6002, doi: 10.1002/2013JB010457.

Drinkwater, M.R., R. Floberghagen, R. Haagmans, D. Muzi, and A. Popescu (2003), GOCE: ESA's first Earth Explorer Core mission, In Earth Gravity Field from Space - from Sensors to Earth Sciences. In the Space Sciences Series of ISSI, Vol. 18, 419-432, *Kluwer Academic Publishers*, Dordrecht, Netherlands.

Featherstone, W. E., C. Hirt, and M. Kuhn (2013), Band-limited Bouguer gravity identifies new basins on the Moon, *Journal Geophysical Research - Planets* 118(6), 1397-1413, doi:10.1002/jgre.20101.

Flury J. (2005), ice mass balance and ice dynamics from satellite gravity missions, *Earth, Moon, and Planets* (2005) 94: 83–91, DOI 10.1007/s11038-004-8213-5.

Forsberg R, A. V Olesen H. Yildiz, C. C. Tscherning (2011), Polar Gravity Fields From Goce And Airborne Gravity, *Proc of 4th International GOCE User Workshop*, Munich, Germany, ESA SP-696, July 2011.

Fretwell, P., Pritchard, H. D., Vaughan, D. G., Bamber, J. L., et al. (2013), Bedmap2: improved ice bed, surface and thickness datasets for Antarctica, *The Cryosphere*, 7, 375-393, doi:10.5194/tc-7-375-2013, 2013.

Grombein, T., Luo, X., Seitz, K., Heck, B. 2014. A wavelet-based assessment of topographic-isostatic reductions for GOCE gravity gradients. *Surveys in Geophysics*, doi: 10.1007/s10712-014-9283-1.

Goossens S., K. Matsumoto, Q. Liu, F. Kikuchi, et al. (2011), Lunar gravity field determination using SELENE same-beam differential VLBI tracking data, *J. Geod., 85*(4), 205-228, doi: 10.1007/s00190-010-0430-2.

Hirt, C., S.J. Claessens, T. Fecher, M. Kuhn, R. Pail, M. Rexer (2013), New ultra-high resolution picture of Earth's gravity field, *Geophysical Research Letters*, 40(16), 4279-4283, doi: 10.1002/grl.50838.

Hirt C, Kuhn M, Featherstone WE, Göttl, F (2012), Topographic/isostatic evaluation of new-generation GOCE gravity field models, *Journal Geophysical Research – Solid Earth*, 117, B05407, doi:10.1029/2011JB008878.

Ivins, E.R. and T.S. James, (2005), Antarctic glacial isostatic adjustment: A new assessment, *Antarctic Science* 17 (4), 541-553.

Konopliv, A.S., Asmar, S.W., Folkner, W.M., Karatekin, Ö., Nunes, D.C., Smrekar, S.E., Yoder, C.F., Zuber, M.T. (2011), Mars high resolution gravity fields from MRO, Mars seasonal gravity, and other dynamical parameters, *Icarus*, 211, 401–428.

Lemoine F.G., S. Goossens, T.J. Sabaka, J.B. Nicholas et al. (2014), GRGM900C: A degree-900 lunar gravity model from GRAIL primary and extended mission data, *Geophysical Research Letters*, doi: 10.1002/2014GL060027.

Lythe, M. B., D. G. Vaughan, *and the Bedmap Consortium*. (2001), BEDMAP: A new ice thickness and subglacial topographic model of Antarctica, *J. Geophys. Res*., 106(B6), 11335–11351, doi:10.1029/2000JB900449.

Moritz, H. (2000), Geodetic Reference System 1980. *J. Geod.*, 74, 128-140.

O'Donnell J.P., and A.A. Nyblade (2014), Antarctica's hypsometry and crustal thickness: Implications for the origin of anomalous topography in East Antarctica, *Earth Planetary Science Letters* 388, 143-155.

Pail, R., S. Bruinsma, F. Migliaccio, C. Förste, et al. (2011), First GOCE gravity field models derived by three different approaches, *J Geod.*, 85(11), 819-843, doi: 10.1007/s00190-011-0467-x.

Papp G (2009), Simultaneous determination of terrain correction and local average topographic density, *Acta Geod.Geoph.Hung*., 44(2), 191-202, doi:10.1556/AGeod.44.2009.2.5.

Pavlis N.K., S.A. Holmes, S.C. Kenyon, and J.K. Factor (2012), The development and evaluation of the Earth Gravitational Model 2008 (EGM2008), *J. Geophys. Res.*, 117, B04406, doi:10.1029/2011JB008916.

Rummel, R, M. Horwath, W. Yi, A. Albertella, W. Bosch, R. Haagmans (2011), GOCE, Satellite Gravimetry and Antarctic Mass Transports, Surv. Geophys. 32(4-5), 643-657, doi: 10.1007/s10712-011-9115-5.

Rummel, R., Rapp, R.H., Sünkel, H., Tscherning, C.C. (1988), Comparisons of global topographic/isostatic models to the Earth's observed gravity field. Report No 388, *Dep. Geodetic Sci. Surv*., Ohio State University, Columbus, Ohio.

Schwabe, J., Scheinert, M., Dietrich, R., Ferracccioli, F., Jordan, T. (2012), Regional geoid improvement over the Antarctic Peninsula Utilizing Airborne Gravity Data. In: Geodesy for Planet Earth, *IAG Conf Series* 136, 457-464, Springer.

Shepherd, A., Ivins ER, Geruo A, Valentina R, et al. (2012), A reconciled estimate of ice sheet mass balance, *Science*, 338, 1183–1189, doi:10.1126/science.1228102.

van der Meijde, M R. Pail, R. Bingham, R. Floberghagen (2013), GOCE data, models, and applications: A review, *International Journal of Applied Earth Observation and Geoinformation*, online first.